An integrated optimal-GICP design for the SPRT control chart with estimated process parameters based on the average number of observations to signal

Quality Technology & Quantitative Management

ISSN: (Print) (Online) Journal homepage: www.tandfonline.com/journals/ttqm20

An integrated optimal-GICP design for the SPRT control chart with estimated process parameters based on the average number of observations to signal

J.W. Teoh, W.L. Teoh, Michael B.C. Khoo, K.P. Tran & M.H. Lee

To cite this article: J.W. Teoh, W.L. Teoh, Michael B.C. Khoo, K.P. Tran & M.H. Lee (07 Feb 2024): An integrated optimal-GICP design for the SPRT control chart with estimated process parameters based on the average number of observations to signal, Quality Technology & Quantitative Management, DOI: 10.1080/16843703.2024.2312010

To link to this article: https://doi.org/10.1080/16843703.2024.2312010

Published online: 07 Feb 2024.

QUALITY TECHNOLOGY & QUANTITATIVE MANAGEMENT
https://doi.org/10.1080/16843703.2024.2312010

Taylor & Francis
Taylor & Francis Group

An integrated optimal-GICP design for the SPRT control chart with estimated process parameters based on the average number of observations to signal

J.W. Teoh [a], W.L. Teoh [a,d], Michael B.C. Khoo [b], K.P. Tran [c,d] and M.H. Lee [e]

[a]School of Mathematical and Computer Sciences, Heriot-Watt University Malaysia, Putrajaya, Malaysia; [b]School of Mathematical Sciences, Universiti Sains Malaysia, Penang, Malaysia; [c]University of Lille, ENSAIT, ULR 2461 – GEMTEX – Génie et Matériaux Textiles, Lille, France; [d]International Chair in Data Science & Explainable Artificial Intelligence, International Research Institute for Artificial Intelligence and Data Science, Dong A University, Danang, Vietnam; [e]Faculty of Engineering, Computing and Science, Swinburne University of Technology Sarawak Campus, Kuching, Malaysia

ABSTRACT

As a variable-sample-size control scheme, the sequential probability ratio test (SPRT) chart is favoured due to its sensitivity and high sampling efficiency. It is frequently documented that the SPRT chart inspects only a small number of observations at each sampling stage, making the said chart extremely appealing to quality engineers. In the current literature, most developments of the SPRT chart are established based on the average run length and average time to signal metrics. However, these metrics do not consider sampling efficiency. In this paper, we develop two optimal designs of the SPRT chart, based on (i) the average value of the average number of observations to signal (AANOS) and (ii) the expected value of the AANOS, with consideration of Phase-I process parameter estimation. We develop a model that integrates the concept of optimization and the guaranteed in-control performance (GICP) framework to neutralize the adverse effects of parameter estimation. Results show that the proposed optimal-GICP design preserves satisfactory out-of-control performances for moderate and large mean shifts, while keeping the false alarm rates at reasonably low levels. Finally, we illustrate an example of the SPRT chart with estimated process parameters for monitoring loop height measurements from a wire bonding dataset.

ARTICLE HISTORY
Received 17 July 2023
Accepted 26 January 2024

KEYWORDS
Average number of observations to signal; guaranteed in-control performance; optimal design; phase-I parameter estimation; SPRT control chart; statistical process monitoring

1 Introduction

Statistical process monitoring (SPM) refers to the procedure of employing statistical techniques to control the stability of a process. The vast majority of manufacturing organizations rely on quality control charts to achieve this aim, as control charts are widely recognized tools for process visualization and fault diagnosis. To date, the SPM community has contributed to countless developments of control charting schemes in multiple avenues, see Khusna et al. (2020), Katebi and Rahim (2021), and Kumar (2022).

The sequential probability ratio test (SPRT) control chart is constructed by applying a sequence of independent SPRTs at fixed time intervals, where each SPRT samples a random

CONTACT W.L. Teoh wei_lin.teoh@hw.ac.uk School of Mathematical and Computer Sciences, Heriot-Watt University Malaysia, Putrajaya, Malaysia

This article has been corrected with minor changes. These changes do not impact the academic content of the article.

number of observations (Stoumbos & Reynolds, 1997). Several researchers, including Ou et al. (2012), Teoh et al. (2022), Mahadik and Godase (2023), showed that the SPRT chart has a superior detection performance over the Shewhart and cumulative sum (CUSUM) charts. To improve the performance of the SPRT chart over a range of process mean shifts, Ou et al. (2012) proposed an optimization algorithm that tunes two charting parameters, i.e. the reference parameter and in-control average sample number (ASN), to achieve the minimum average extra quadratic loss (AEQL). Though the design becomes slightly more complex, the resulting optimal SPRT chart harvests an improvement in its weighted performance by over 100% compared to the basic SPRT chart. Besides, the SPRT is widely employed in various industrial applications, such as monitoring the breaking strength of strapping tapes (Chou et al., 2006), monitoring the urinary glycosaminoglycan concentration of children aged below 17 years (Godase et al., 2022), testing the failure times of electrical insulating fluids (Rasay & Alinezhad, 2022), and monitoring the tensile strength of polyester resins (Mahadik & Godase, 2023).

Traditional control chart designs, which assume that the process parameters (i.e. mean and standard deviation) are known, are no longer relevant in practice. Modern designs are mostly built upon the assumption that the process parameters are estimated, see for example, Saleh et al. (2015), Hu and Castagliola (2019), Sarmiento et al. (2022), and Teoh et al. (2022). Capizzi and Masarotto (2020) pointed out that, in many modern manufacturing systems, production often transits between various products for a number of reasons, some of which include the dynamic nature of market trends, evolving customer preferences, technological advancements, and changes in the supply chain. Typical examples can be found in the production of customized mechanical devices and fashionable clothes, where changes in the product design often serve as a strategic move to improve the competitiveness of a firm. For this reason, historical data characterizing the quality of such products can be limited in amount, and they are often inadequate in supporting the accurate estimation of the Phase-I process parameters. Many scholars, including Hu and Castagliola (2019), Sarmiento et al. (2022), and Teoh et al. (2022), have revealed that a small number of Phase-I observations can result in extremely volatile parameter estimates, as well as excessive false alarms during the operation of the control chart with estimated process parameters. Teoh et al. (2022) discovered that, by using the traditional SPRT chart, practitioners have a near 50% risk of obtaining false alarm rates exceeding the recommended threshold when the process parameters were estimated. This observation is deemed endangering to the long run growth of a business, as massive false alarms can reduce productivity and destroy the inspectors' confidence. As a remedial measure, the guaranteed in-control performance (GICP) framework has been introduced for designing control charts with estimated process parameters, see for example, Khusna et al. (2020), Kumar (2022), Sarmiento et al. (2022), and Gong et al. (2023). The GICP design has been widely recognized as the most robust and effective method to replace the traditional design of control charts with estimated process parameters. Kumar (2022) demonstrated that, by adjusting the control limits using the expected probability criterion (EPC), the practitioner is guaranteed a high probability of obtaining an in-control conditional run length exceeding a specified threshold, even when a small number of Phase-I samples is used. Based on a review by Sarmiento et al. (2022), the GICP design is said to be consistent with the risk limiting philosophy, and such a design can lead to better-controlled false alarm rates, which in turn leads to reduced wastage in terms of labour, time, and materials. However, as shown by Saleh et al. (2015), Kumar (2022), and Sarmiento et al. (2022), the GICP can lead to a reduction in the chart's sensitivity towards small and moderate process deviations. This implies that, even though a desired in-control performance is guaranteed, the control chart may lose part of its detection ability as a result of an inflated control limit. Recently, Teoh et al. (2022) proposed a new GICP framework coupled with an optimization design based on the AEQL. They showed that the proposed optimal-GICP design is effective in reducing the trade-off between the in-control and out-of-control performances, resolving the main drawback of the GICP design.

In the existing designs of control charts, most researchers place a major emphasis on optimizing the average run length (ARL) or average time to signal (ATS) metric. However, both of these metrics ignore the average sample size, which is an important characteristic for variable-sample-size-type (VSS) charts, such as the SPRT chart. Several researchers, including You et al. (2015), Godase and Mahadik (2019), Katebi and Rahim (2021), and Deore et al. (2023) suggested the average number of observations to signal (ANOS) metric as an alternative metric for evaluating the performance of VSS control charts. They argued that the ANOS is a more meaningful metric as it combines both the run length information and the sampling efficiency, hence providing a more accurate measure for the effectiveness of a VSS control chart. Godase and Mahadik (2019) and Deore et al. (2023) showed that, in addition to the ARL performance, the SPRT chart offers a comparable performance against the cumulative sum (CUSUM) and exponentially weighted moving average (EWMA) control charts in terms of the ANOS.

While Godase and Mahadik (2019) and Deore et al. (2023) had proven significant success with their proposed SPRT chart, it is worth noting that their design methodology assumes that the shift size was known *a priori*. This design would have been effective if practitioners had a specialised understanding of the level of shift, to which a process is likely to move. However, in practice, practitioners often have limited knowledge about the critical shift in a production process, which makes the design of control charts immensely challenging. Many researchers, such as Ou et al. (2012), Calzada and Scariano (2013), and Chong et al. (2022) have pointed out that, if the actual process shift size differs from the shift size used in the design of control charts, the chart's performance would change drastically from the intended level. This implies that deviations of an industrial process from its original mean are more likely to go unnoticed, which in turn leads to huge scrap and rework costs. To rectify the problem, scholars have proposed designing the control charts by optimizing their performances over a range of unknown shift sizes, see for example, Calzada and Scariano (2013), Malela-Majika et al. (2021), Mustafa et al. (2023), Yeong et al. (2023). These designs typically use an 'average' metric of the performance values, e.g. expected value of the ARL, expected value of the ANOS, AEQL, etc., as the objective function for the optimization model. It is found that these metrics are more representative of the overall performance of a control chart across a domain of shift sizes, hence facilitating better decision-making and parameter selection during the design of control charts. In this paper, we extend the work of Teoh et al. (2022) by developing two integrated optimal-GICP designs for the SPRT chart with estimated process parameters, based on (i) the average of the ANOS (AANOS) assuming that shift sizes are deterministic, and (ii) the expected value of the AANOS (EAANOS) assuming that shift sizes are unknown. Both designs are useful as they address the different needs of a practitioner.

The remainder of the paper is structured as follows. Section 2 details the theoretical formulations of the SPRT chart with known and unknown process parameters. New formulae for the AANOS and standard deviation of the ANOS (SDANOS) are also derived. Section 3 presents some preliminary results comparing the performances of the SPRT chart with known and estimated process parameters. Section 4 details two new algorithms for constructing the optimal SPRT chart with estimated process parameters, in cases where shift sizes are deterministic and unknown, respectively. Section 5 illustrates the implementation of the proposed optimal SPRT chart with a real industrial dataset. Some concluding remarks and future work are discussed in Section 6.

2 The SPRT control chart

2.1 Run-length properties of the SPRT chart with known process parameters

Define a random variable X whose distribution is normal with known mean μ_0 and standard deviation σ_0. The SPRT chart examines a sequence of observations corresponding to N_i, i.e.

$\left(X_{1,1}, X_{1,2} \ldots, X_{1,N_1}\right)$, $\left(X_{2,1}, X_{2,2} \ldots, X_{2,N_2}\right)$, ... , where N_i represents the number of observations required to conclude the i^{th} SPRT, for $i = 1, 2, \ldots$. A signal is produced when it detects a change in the process mean from $\mu = \mu_0$ to $\mu = \mu_0 + \delta\sigma_0$, where δ is the size of the mean shift. Each observation is assumed to be sampled independently within an insignificant amount of time. The upper-sided ($C_{i,j}^{+}$) and lower-sided ($C_{i,j}^{-}$) charting statistics of the SPRT chart with known process parameters can be calculated using

$$C_{i,j}^{+} = \sum\nolimits_{\theta=1}^{j} \left(Z_{i,\theta} - \gamma\right) \tag{1}$$

and

$$C_{i,j}^{-} = \sum\nolimits_{\theta=1}^{j} \left(Z_{i,\theta} + \gamma\right), \tag{2}$$

respectively, where $Z_{i,\theta} = \left(X_{i,\theta} - \mu_0\right)/\sigma_0$ and $\gamma > 0$ is the reference value. Here, $i = 1, 2, \ldots$ represents the number of SPRT's and $j = 1, 2, \ldots, N_i$ represents the observation number of the i^{th} SPRT.

The decision rule for each SPRT is governed by two control limits, g and h. For the upper-sided SPRT chart, (g, h) represent the acceptance and rejection limits, respectively, whereas for the lower-sided SPRT chart, the acceptance and rejection limits are $(-g, -h)$, respectively. In particular,

- when $C_{i,j}^{+} > h\left(C_{i,j}^{-} < -h\right)$, the process is signalled as out-of-control with a probable upward (downward) mean shift,
- when $C_{i,j}^{+} < g\left(C_{i,j}^{-} > -g\right)$, the process is indicated as in-control,
- when $g \le C_{i,j}^{+} \le h\left(-h \le C_{i,j}^{-} \le -g\right)$, sampling continues until either of the charting statistics falls beyond the control limits.

Note that the upper-sided and lower-sided SPRT charts are symmetric, hence, they possess identical run-length properties. Without loss of generality, we only consider the mechanism of the upper-sided SPRT chart and its run-length properties in this section.

The efficiency of the upper-sided SPRT chart with known process parameters is measured by its ASN. By means of the Markov chain approach, the ASN can be evaluated as the average number of steps within the region $[g, h]$ before the charting statistic lands on either the acceptance or the rejection state. We first divide $[g, h]$ into D subintervals of width $\Delta = (h - g)/D$, then define each subinterval as a transient state S_k, for $k = 1, \ldots, D$. The ASN can be evaluated using the following matrix-vector equation

$$\text{ASN} = \mathbf{B}^{\text{T}}(\mathbf{I} - \mathbf{Q})^{-1}1 + 1, \tag{3}$$

where $\mathbf{B}$ is a $D \times 1$ vector of initial transition probabilities, $\mathbf{Q}$ is a $D \times D$ one-step transition probability matrix, $1 = (1, 1, \ldots, 1)^{\text{T}}$ and $\mathbf{I}$ is a $D \times D$ identity matrix. The expressions for the entries of $\mathbf{Q}$ ($q_{k,\ell}$) and $\mathbf{B}$ (b_k) are given as

$$q_{k,\ell} = \Phi[\gamma + (\ell - k + 0.5) \cdot \Delta - \delta] - \Phi[\gamma + (\ell - k - 0.5) \cdot \Delta - \delta] \tag{4}$$

and

$$b_k = \Phi(\gamma + k \cdot \Delta + g - \delta) - \Phi[\gamma + (k - 1) \cdot \Delta + g - \delta], \tag{5}$$

respectively, for $k, \ell = 1, 2, \ldots, D$, where $\Phi(\cdot)$ is the cumulative distribution function of the standard normal distribution.

To compute the ARL of the SPRT chart, one needs to first find the probability that the SPRT is in-control. This probability is known as the operating characteristic (OC) function, and its expression is

$$\mathrm{OC} = P_0 + \mathbf{B}^{\mathrm{T}}(\mathbf{I} - \mathbf{Q})^{-1}\mathbf{R}. \tag{6}$$

Here, P_0 is the one-step probability that the initial charting statistic falls into the acceptance state, and $\mathbf{R}$ is a $D \times 1$ vector of one-step transition probabilities from state S_k to the acceptance state. The expressions for P_0 and the entries of $\mathbf{R}$ (r_k) are given as

$$P_0 = \Phi(\gamma + g - \delta) \tag{7}$$

and

$$r_k = \Phi[\gamma + (0.5 - k) \cdot \Delta - \delta], \tag{8}$$

respectively. Stoumbos and Reynolds (1997) derived the ARL of the SPRT chart as

$$\mathrm{ARL} = \frac{1}{1 - \mathrm{OC}}, \tag{9}$$

using the first moment of a geometric distribution. They also showed that the ANOS of the SPRT chart is equal to

$$\mathrm{ANOS} = \mathrm{ARL} \times \mathrm{ASN}, \tag{10}$$

which obeys Wald's Identity (Godase & Mahadik, 2019).

It is useful to quantify the average ANOS performance of the SPRT chart over a specified range of process mean shifts $[\delta_{\min}, \delta_{\max}]$, i.e. to calculate the expected value of the ANOS (EANOS), using the integral formula below:

$$\mathrm{EANOS} = \int_{\delta_{\min}}^{\delta_{\max}} \mathrm{ANOS}\, f_\delta(\delta) d\delta, \tag{11}$$

where $f_\delta(\delta)$ is the probability density function (pdf) of the shift size δ, while $\delta_{\min}$ and $\delta_{\max}$ are the minimum and maximum mean shifts, respectively. Calzada and Scariano (2013) and Yeong et al. (2023) ascertained that the distribution of the shift size δ is almost uncertain in practice, hence, it is reasonable to take $f_\delta(\delta)$ as the pdf of the uniform distribution over the shift range $[\delta_{\min}, \delta_{\max}]$. The EANOS can be simplified from Equation (11) as

$$\mathrm{EANOS} = \frac{1}{\delta_{\max} - \delta_{\min}} \int_{\delta_{\min}}^{\delta_{\max}} \mathrm{ANOS}\, d\delta. \tag{12}$$

2.2 Run-length properties of the SPRT chart with unknown process parameters

Prior to Phase-II monitoring, the mean and standard deviation of the process need to be estimated from a set of in-control Phase-I samples $(Y_1, Y_2, \ldots, Y_m)$. Common estimators for the mean μ_0 and standard deviation σ_0 are

$$\hat{\mu}_0 = \frac{\sum_{\varphi=1}^{m} Y_\varphi}{m} \tag{13}$$

and

$$\hat{\sigma}_0 = \sqrt{\frac{\sum_{\varphi=1}^{m} \left(Y_\varphi - \hat{\mu}_0\right)^2}{m - 1}}, \tag{14}$$

respectively. Using $\hat{\mu}_0$ and $\hat{\sigma}_0$ in place of the true process parameters, the upper- and lower-sided charting statistics in Equations (1) and (2) can be modified as

$$\hat{C}_{i,j}^{+} = \sum_{\theta=1}^{j} \left(\hat{Z}_{i,\theta} - \gamma\right) \tag{15}$$

and

$$\hat{C}_{i,j}^{-} = \sum_{\theta=1}^{j} \left(\hat{Z}_{i,\theta} + \gamma\right), \tag{16}$$

respectively, where $\hat{Z}_{i,\theta} = \left(X_{i,\theta} - \hat{\mu}_0\right)/\hat{\sigma}_0$.

The run-length properties of the SPRT chart with estimated process parameters now depend on the quantities defined in Equations (13) and (14). Defining $U = \left(\hat{\mu}_0 - \mu_0\right)/(\sigma_0/\sqrt{m})$ and $V = \hat{\sigma}_0/\sigma_0$, we can express the run-length properties as conditional functions of U and V. It is known that U follows the standard normal distribution, whereas V follows a distribution with the following pdf

$$f_V(v) = 2(m-1)v f_{\chi^2,m-1}\left[(m-1)v^2\right].$$

Here, $f_{\chi^2,m-1}(\cdot)$ is the pdf of the chi-square distribution with $m-1$ degrees of freedom.

When process parameters are estimated, the expressions for the ASN, ARL, and ANOS of the SPRT chart are replaced by the conditional ASN (CASN), conditional ARL (CARL), and conditional ANOS (CANOS), respectively. The CASN of the SPRT chart with estimated process parameters is modified from Equation (3) as

$$\text{CASN} = \hat{\mathbf{B}}^{\mathrm{T}}\left(\mathbf{I} - \hat{\mathbf{Q}}\right)^{-1}1 + 1, \tag{17}$$

where the entries of $\widehat{\mathbf{Q}}$ ($\hat{q}_{k,\ell}$) and $\widehat{\mathbf{B}}$ ($\hat{b}_k$) can be modified from Equations (4) and (Eq 5) as

$$\hat{q}_{k,\ell} = \Phi\left[V(\gamma + (\ell - k + 0.5)\cdot\Delta\ ) + \frac{U}{\sqrt{m}} - \delta\right] - \Phi\left[V(\gamma + (\ell - k - 0.5)\cdot\Delta\ ) + \frac{U}{\sqrt{m}} - \delta\right] \tag{18}$$

and

$$\hat{b}_k = \Phi\left[V(\gamma + k\cdot\Delta\ + g) + \frac{U}{\sqrt{m}} - \delta\right] - \Phi\left[V(\gamma + (k-1)\cdot\Delta\ + g) + \frac{U}{\sqrt{m}} - \delta\right], \tag{19}$$

respectively.

The CARL of the SPRT chart with estimated process parameters can be evaluated using a method similar to the known-parameter case. The operating characteristic function with estimation errors $\widehat{\text{OC}}$ is modified from Equation (6) as

$$\widehat{\text{OC}} = \hat{P}_0 + \widehat{\mathbf{B}}^{\mathrm{T}}\left(\mathbf{I} - \widehat{\mathbf{Q}}\right)^{-1}\widehat{\mathbf{R}}, \tag{20}$$

where $\hat{P}_0$ and the entries of vector $\widehat{\mathbf{R}}$ ($\hat{r}_k$) can be modified from Equations (7) and (8) as

$$\hat{P}_0 = \Phi\left[V(\gamma + g) + \frac{U}{\sqrt{m}} - \delta\right] \tag{21}$$

and

$$\hat{r}_k = \Phi\left[V(\gamma + (0.5 - k)\cdot\Delta\ ) + \frac{U}{\sqrt{m}} - \delta\right], \tag{22}$$

respectively. The CARL and CANOS are therefore modified from Equations (9) and (10) as

$$\text{CARL} = \frac{1}{1 - \widehat{\text{OC}}} \tag{23}$$

and

$$\text{CANOS} = \text{CARL} \times \text{CASN}, \tag{24}$$

respectively, where $\widehat{\text{OC}}$ is quoted directly from Equation (20).

While the CASN, CARL, and CANOS are useful measures of the chart's performances for a specific set of $(\hat{\mu}_0, \hat{\sigma}_0)$, their interpretability is quite restricted in the sense that the performances across all parameter estimates are not reflected. To take into account all the parameter estimates, one suitable approach is to evaluate their unconditional properties by averaging the functions over the joint distributions of U and V. In particular, the expected value of the CASN (AASN) can be found as

$$\text{AASN} = \text{E}[\text{CASN}] = \int_0^\infty \int_{-\infty}^\infty \text{CASN} f_U(u) f_V(v)\, du\, dv, \tag{25}$$

where $f_U(\cdot)$ and $f_V(\cdot)$ are the pdfs of U and V, respectively, and CASN can be quoted directly from Equation (17).

Since the central premise of this paper encompasses optimal designs based on the ANOS, we only derive unconditional properties of the CANOS. The expected value (AANOS) and standard deviation (SDANOS) of the CANOS are derived as

$$\text{AANOS} = \text{E}[\text{CANOS}] = \int_0^\infty \int_{-\infty}^\infty \text{CANOS} f_U(u) f_V(v)\, du\, dv \tag{26}$$

and

$$\begin{aligned}\text{SDANOS} &= \sqrt{\text{E}\left[\text{CANOS}^2\right] - (\text{E}[\text{CANOS}])^2} \\ &= \sqrt{\int_0^\infty \int_{-\infty}^\infty \text{CANOS}^2 f_U(u) f_V(v) du dv - \text{AANOS}^2},\end{aligned} \tag{27}$$

respectively, where the expression for CANOS can be quoted from Equation (24). The expected value of the EANOS (EAANOS) over a range of mean shifts $\delta \in [\delta_{\min}, \delta_{\max}]$ is derived as

$$\begin{aligned}\text{EAANOS} &= \int_{\delta_{\min}}^{\delta_{\max}} \int_0^\infty \int_{-\infty}^\infty \text{CANOS} f_U(u) f_V(v) f_\delta(\delta) du\, dv\, d\delta \\ &= \frac{1}{\delta_{\max} - \delta_{\min}} \int_{\delta_{\min}}^{\delta_{\max}} \int_0^\infty \int_{-\infty}^\infty \text{CANOS} f_U(u) f_V(v) du\, dv\, d\delta.\end{aligned} \tag{28}$$

3 The effect of Phase-I parameter estimation on the performances of the SPRT chart with unadjusted control limits

This section compares the performances of the SPRT chart designed under the traditional method, in cases when process parameters are known and estimated. Teoh et al. (2022) showed that, even with a large Phase-I sample size m, the practitioner is still susceptible to a 50% risk of obtaining false alarm rates higher than the recommended rate. To date, most of these inferences were made upon the CARL, and none was made upon the CANOS. In this section, we investigate the conditional and unconditional properties of the CANOS of the SPRT chart when different m values are adopted.

Three performance metrics are considered in this section, i.e. the AANOS, SDANOS, and the exceedance probability $\Pr(\text{CANOS}_0 \geq \tau)$. Here, CANOS_0 refers to the in-control CANOS (i.e. when $\delta = 0$), and τ is the minimum recommended CANOS_0. In this study, the SPRT chart is

designed by minimizing the EANOS (see Equation (12)) corresponding to the case of known process parameters. The developed optimization algorithm determines the optimal charting parameters (γ, g, h) that yields the smallest EANOS value, subject to the constraints $\text{ANOS}_0 = \tau$ and $\text{ASN}_0 = \bar{n}$. Here, ASN_0 is the in-control ASN and $\bar{n}$ is the desired value of ASN_0. In our demonstration, we set the design specifications as $(\tau, \bar{n}, \delta_{\min}, \delta_{\max}) = (1500, 5, 0.1, 2.0)$. By implementing a similar optimization algorithm detailed in Ou et al. (2010), the design parameters for the optimal SPRT chart with known process parameters are computed as $(\gamma, g, h) = (0.164, -0.122, 12.427)$.

Table 1 shows the three performance indicators of the unadjusted SPRT chart with estimated process parameters ($m \in \{50, 100, 200, 400, 600, 1000, 2000\}$) and known process parameters ($m = +\infty$), for mean shifts $\delta \in \{0.0, 0.2, 0.4, 0.6, 0.8, 1.0, 1.5, 2.0\}$. The topmost row of the table reveals the Phase-I sample size m. The subsequent two rows show the $\Pr(\text{CANOS}_0 \geq \tau)$ and $(\text{AANOS}, \text{SDANOS})$ values, respectively. As a numeric example, when $m = 400$, the exceedance probability $\Pr(\text{CANOS}_0 \geq \tau)$ is 49.55%, and the out-of-control AANOS (AANOS_1) and SDANOS (SDANOS_1) values at $\delta = 0.2$ are 156.94 and 81.91, respectively (see Table 1). The values of AANOS and SDANOS are calculated using Equations (26) and (27), respectively, whereas $\Pr(\text{CANOS}_0 \geq \tau)$ is approximated by simulating 100,000 CANOS_0 values using Equation (24). Note that when $m = +\infty$, the SDANOS equals zero for all values of δ.

From the conditional perspective, one observes that the $\Pr(\text{CANOS}_0 \geq \tau)$ values are lower than 50% even for a reasonably large m (= 2000). This is an alarming sign, especially when the ASN_0 value is fixed, as the user faces a high risk of encountering more false alarms than usual over the course of monitoring. Excessive false alarms associated with low exceedance probabilities can lead to wastage, increased procedural costs, and declined productive efficiency. Therefore, it is essential to develop a design strategy that keeps the average false alarm rate at a low level (i.e. maintains the exceedance probability at a high level). From the unconditional viewpoint, the AANOS values converge to the ANOS value in the known-parameter case as m increases. As m increases, the

Table 1. $\Pr(\text{CANOS}_0 \geq \tau)$, AANOS, and SDANOS values for the SPRT chart with optimal charting parameters (γ, g, h) = (0.164, −0.122, 12.427) obtained from minimizing the EANOS corresponding to the case of known process parameters, when $\text{ASN}_0 = 5$, $\text{ANOS}_0 = \tau = 1500$, $\delta_{\min} = 0.1$, $\delta_{\max} = 2.0$, and $m \in \{50, 100, 200, 400, 600, 1000, 2000, +\infty\}$.

	$m = 50$	$m = 100$	$m = 200$	$m = 400$
δ	$\Pr(\text{CANOS}_0 \geq \tau)$ (AANOS, SDANOS)	$\Pr(\text{CANOS}_0 \geq \tau)$ (AANOS, SDANOS)	$\Pr(\text{CANOS}_0 \geq \tau)$ (AANOS, SDANOS)	$\Pr(\text{CANOS}_0 \geq \tau)$ (AANOS, SDANOS)
	48.69%	49.10%	49.38%	49.55%
0.0	(>100,000, >1,000,000)	(>10,000, >100,000)	(4156.03, >10,000)	(2381.83, 3216.20)
0.2	(5427.70, >500,000)	(329.86, 3220.44)	(187.63, 216.27)	(156.94, 81.91)
0.4	(96.11, >10,000)	(57.15, 44.12)	(52.02, 16.53)	(50.20, 10.01)
0.6	(32.17, 35.32)	(29.99, 8.04)	(29.23, 5.05)	(28.90, 3.40)
0.8	(21.16, 6.01)	(20.63, 3.75)	(20.40, 2.53)	(20.30, 1.75)
1.0	(16.00, 3.40)	(15.80, 2.27)	(15.71, 1.57)	(15.66, 1.10)
1.5	(10.07, 1.51)	(10.04, 1.05)	(10.02, 0.73)	(10.01, 0.52)
2.0	(7.41, 0.93)	(7.41, 0.65)	(7.40, 0.46)	(7.40, 0.32)
	$m = 600$	$m = 1000$	$m = 2000$	$m = +\infty$
δ	$\Pr(\text{CANOS}_0 \geq \tau)$ (AANOS, SDANOS)	$\Pr(\text{CANOS}_0 \geq \tau)$ (AANOS, SDANOS)	$\Pr(\text{CANOS}_0 \geq \tau)$ (AANOS, SDANOS)	$\Pr(\text{CANOS}_0 \geq \tau)$ ANOS
	49.66%	49.68%	49.81%	100%
0.0	(2021.68, 1874.11)	(1785.97, 1136.14)	(1633.97, 677.17)	1500
0.2	(149.34, 57.30)	(143.93, 39.76)	(140.22, 26.06)	136.77
0.4	(49.66, 7.83)	(49.25, 5.88)	(48.96, 4.06)	48.67
0.6	(28.79, 2.74)	(28.71, 2.10)	(28.65, 1.47)	28.59
0.8	(20.26, 1.42)	(20.23, 1.09)	(20.21, 0.77)	20.19
1.0	(15.64, 0.89)	(15.63, 0.69)	(15.62, 0.49)	15.62
1.5	(10.01, 0.42)	(10.01, 0.33)	(10.01, 0.23)	10.00
2.0	(7.40, 0.26)	(7.40, 0.20)	(7.40, 0.14)	7.40

SDANOS values tend to zero, indicating reduced variability in the CANOS distributions for larger sample sizes. It is also noticed that Phase-I parameter estimation has little impact on the performance of the SPRT chart when δ is moderate or large. In particular, when $\delta \geq 0.6$, the AANOS_1 values of the SPRT chart with estimated process parameters are justifiably close to the nominal out-of-control ANOS (ANOS_1) values, for m as small as 50.

4 Optimization framework based on the GICP method

In this section, we introduce optimal designs of the SPRT chart with estimated process parameters under the GICP framework by minimizing (i) AANOS_1 and (ii) EAANOS for known and unknown shift sizes, respectively. The GICP method ensures that the exceedance probability does not fall below a specified level, say 90% or 95%. The complete formulation of the GICP framework for the CANOS_0 based on the EPC is as follows:

$$\Pr[\text{CANOS}_0 \geq (1-\varepsilon)\tau] = 1 - p, \tag{29}$$

where p is the risk probability and ε is a tolerance term. The value of p is specified as a small percentage (e.g. 5%), and it represents the proportion of practitioners at risk of obtaining an undesirably small CANOS_0 value. ε is introduced to lower the threshold and allow for a more flexible in-control policy. It is worth noting that Equation (29) may lead to either:

(1) a large in-control CARL (CARL_0) and a small in-control CASN (CASN_0), or
(2) a small CARL_0 and a large CASN_0, or
(3) both large CARL_0 and CASN_0,

since $\text{CANOS}_0 = \text{CARL}_0 \times \text{CASN}_0$. While a large CARL_0 value is favorable, the practitioner may wish to avoid a large CASN_0 to improve the long-run efficiency of the system. It is therefore clear that consequences (2) and (3) are undesirable. To tackle problems that might arise from the GICP model, the value of the in-control AASN (AASN_0) is fixed throughout the optimization design. This ensures that the incidence of the EPC mainly falls on the CARL_0 rather than the CASN_0.

Sections 4.1 and 4.2 present two optimization models for the SPRT chart with estimated process parameters based on the AANOS_1 and EAANOS metrics, respectively. In Section 4.1, it is assumed that practitioner has a sophisticated understanding of the underlying manufacturing system, which includes prior knowledge of the probable shift size. Hence, minimizing the AANOS_1 value would imply that both the average of the out-of-control CARL (AARL_1) and the out-of-control AASN (AASN_1) are generally small at a particular shift point. In Section 4.2, we assume that process shifts occur sparsely in practice, and there is no way to predict the actual distribution of the shift sizes. Hence, we adopt the EAANOS metric for a selected range of mean shifts as the objection function of the optimization model.

4.1 Minimizing the AANOS_1 for deterministic shift sizes

The optimal design for the SPRT chart with estimated process parameters is described as follows:

$$\text{Minimize}_{(\gamma,g,h)}\ \text{AANOS}_1, \tag{30a}$$

subject to

$$\Pr[\text{CANOS}_0 \geq (1-\varepsilon)\tau] = 1 - p, \tag{30b}$$

and

$$\text{AASN}_0 = \bar{n}. \tag{30c}$$

Note that constraint (30b) coincides with the EPC formulation defined in Equation (29). The flow of the AANOS-optimization algorithm is as follows: the user first inputs the design specifications, and then specify the objective function (i.e. Equation (30a)) and the relevant constraints to be met (i.e. Equations (30b) and (30c)). The optimal values of (γ, g, h) are then computed to achieve the minimum AANOS_1 value for a specified shift size. The step-by-step procedure for determining the optimal charting parameters is given below:

Step 1: Input the values of $m, \tau, \bar{n}, \delta_{\text{opt}}, p$, and ε, where δ_{opt} is the shift size in the mean for which a quick detection is required.

Step 2: Search γ in the range of $(0, +\infty)$ using the golden section search algorithm. For each γ, search the values of (g, h). In particular, adjust h to satisfy constraint Equation (30b) using the stochastic approximation algorithm. Then, adjust g to satisfy constraint Equation (30c) using a hybrid Newton method. The algorithm is terminated when both g and h converge. In this step, all the possible combinations of (γ, g, h) for $\delta = 0$ are computed. Note that the AASN_0 is computed from Equation (25) by setting $\delta = 0$.

Step 3: Given δ_{opt}, determine the optimal charting parameters (γ, g, h) that yield the smallest AANOS_1 value. Note that the AANOS_1 is computed from Equation (26).

Table 2 tabulates the optimal charting parameters of the SPRT chart designed using the model defined in Equations (30a) to (30c), and their corresponding AANOS_1 and SDANOS_1 values, for $\delta_{\text{opt}} \in \{0.2, 0.4, 0.6, 0.8, 1.0, 1.5, 2.0\}$. The design specifications used are $\tau = 1500$, $\bar{n} = 5$, $p \in \{0.05, 0.10\}$, and $\varepsilon = 0.2$. Teoh et al. (2022) suggested to use at least $m = 200$ samples in Phase-I parameter estimation to avoid dubious results being produced by the optimization procedure. Therefore, in Table 2, we present results for $m \in \{200, 400, 600, 1000, 2000\}$. For each δ_{opt}, the optimal charting parameters (γ, g, h) are given in the first row of each cell, whereas the $(\text{AANOS}_1, \text{SDANOS}_1)$ values are given in the second row. As an example, from Table 2, when $p = 0.10, m = 600$, and $\delta_{\text{opt}} = 0.8$, the optimal charting parameters are determined as $(\gamma, g, h) = (0.407, -1.347, 6.744)$, and the corresponding (AANOS_1, SDANOS_1) values are computed as $(17.72, 1.86)$ (see Table 2).

Three key observations can be made based on the results tabulated in Table 2. First, for each δ_{opt}, the optimum AANOS_1 and SDANOS_1 values show decreasing trends as m increases. When δ_{opt} is small (i.e. 0.2), one observes significant differences in the $(\text{AANOS}_1, \text{SDANOS}_1)$ values between the SPRT chart designed using a small m ($= 200$) and a large m ($= 2000$). The performances are, however, less affected by small m when δ_{opt} is moderate or large (≥ 0.6). Second, the out-of-control performances of the optimal SPRT chart with GICP-adjusted limits can be improved by using a larger p. For instance, when $m = 2000$ and $\delta_{\text{opt}} = 0.6$, the $(\text{AANOS}_1, \text{SDANOS}_1)$ values decrease from (27.51, 1.92) to (26.80, 1.80) when p is increased from 5% to 10%. Similar observations have been reported by other researchers (see, Diko et al., 2019; Teoh et al., 2022), and they recommended adjusting p based on suitable in-control measures. Third, there is a noticeable relationship between δ_{opt} and the γ value of the AANOS-optimal SPRT chart. By referring to Table 2, we find that the optimal γ is approximately $\delta_{\text{opt}}/2$. This observation is consistent with the optimality theorem of Page's procedure, which forms an important basis for the development of the CUSUM control chart (Moustakides, 1986). The only exception occurs when $m = 200$ and $\delta_{\text{opt}} = 0.2$, where the optimization algorithm converges to around $\gamma = 0.2$.

Many scholars have demonstrated the superiority of the SPRT chart over the Shewhart-type control charts and other memory-type control charts (see Deore et al., 2023; Godase & Mahadik, 2019; Ou et al., 2012). To add value to our research work, we provide some illustrations comparing the conditional out-of-control performances of the SPRT, CUSUM, and Shewhart $\bar{X}$ charts with estimated process parameters. Figures 1 and 2 display boxplots of the out-of-control CARL (CARL_1) and CANOS (CANOS_1), respectively, for the SPRT, CUSUM, and Shewhart $\bar{X}$ charts, designed for 200 Phase-I observations, $p = 0.05$, and $\varepsilon = 0.2$. Both figures reveal the CARL_1 and CANOS_1 distributions of the three control charts for four different sizes of mean

Table 2. Optimal charting parameters (γ, g, h) and the corresponding optimum $AANOS_1$ and $SDANOS_1$ values of the SPRT chart with estimated process parameters, designed under the GICP framework, when $p \in \{0.05, 0.10\}$, $\varepsilon = 0.2$, $AASN_0 = 5$, $\tau = 1500$, $m \in \{200, 400, 600, 1000, 2000\}$, and $\delta_{opt} \in \{0.2, 0.4, 0.6, 0.8, 1.0, 1.5, 2.0\}$.

	$m = 200$	$m = 400$	$m = 600$	$m = 1000$	$m = 2000$
	(γ, g, h)	(γ, g, h)	(γ, g, h)	(γ, g, h)	(γ, g, h)
δ_{opt}	($AANOS_1$, $SDANOS_1$)	($AANOS_1$, $SDANOS_1$)	($AANOS_1$, $SDANOS_1$)	($AANOS_1$, $SDANOS_1$)	($AANOS_1$, $SDANOS_1$)
$p = 0.05$					
0.2	(0.285, −0.666, 11.899)	(0.120, 0.336, 23.358)	(0.126, 0.234, 20.007)	(0.123, 0.214, 18.475)	(0.112, 0.259, 17.905)
	(867.46, 2320.70)	(293.90, 301.09)	(225.44, 109.51)	(186.34, 55.19)	(158.66, 28.17)
0.4	(0.237, −0.387, 14.561)	(0.224, −0.381, 13.135)	(0.213, −0.342, 12.831)	(0.217, −0.388, 11.841)	(0.212, −0.375, 11.375)
	(89.56, 50.95)	(68.85, 18.12)	(62.64, 12.08)	(57.59, 8.23)	(53.35, 5.12)
0.6	(0.328, −0.896, 10.239)	(0.323, −0.916, 9.230)	(0.324, −0.938, 8.777)	(0.317, −0.918, 8.526)	(0.316, −0.922, 8.181)
	(37.70, 10.38)	(32.40, 5.57)	(30.63, 4.17)	(28.95, 2.92)	(27.51, 1.92)
0.8	(0.407, −1.299, 8.107)	(0.422, −1.408, 7.037)	(0.424, −1.427, 6.726)	(0.430, −1.464, 6.370)	(0.412, −1.389, 6.387)
	(21.61, 4.24)	(19.26, 2.60)	(18.42, 2.01)	(17.65, 1.48)	(16.93, 0.96)
1.0	(0.531, −1.897, 6.016)	(0.508, −1.815, 5.781)	(0.508, −1.825, 5.560)	(0.515, −1.866, 5.275)	(0.506, −1.832, 5.180)
	(14.07, 2.45)	(12.83, 1.46)	(12.34, 1.13)	(11.89, 0.85)	(11.48, 0.56)
1.5	(0.776, −3.058, 3.794)	(0.781, −3.099, 3.496)	(0.762, −3.017, 3.479)	(0.777, −3.097, 3.288)	(0.750, −2.975, 3.323)
	(6.37, 0.85)	(5.96, 0.55)	(5.78, 0.42)	(5.62, 0.32)	(5.47, 0.21)
2.0	(1.021, −4.212, 2.678)	(1.010, −4.178, 2.527)	(1.024, −4.247, 2.410)	(1.016, −4.218, 2.362)	(1.004, −4.166, 2.328)
	(3.65, 0.40)	(3.44, 0.26)	(3.36, 0.21)	(3.29, 0.16)	(3.21, 0.11)
$p = 0.10$					
0.2	(0.219, −0.297, 13.911)	(0.123, 0.281, 20.036)	(0.107, 0.363, 20.530)	(0.119, 0.229, 17.604)	(0.112, 0.248, 17.090)
	(536.48, 1546.39)	(237.16, 180.18)	(196.08, 81.93)	(168.49, 46.96)	(149.68, 25.86)
0.4	(0.218, −0.288, 14.041)	(0.215, −0.340, 12.583)	(0.217, −0.376, 11.840)	(0.211, −0.351, 12.145)	(0.215, −0.394, 10.945)
	(76.70, 36.04)	(62.78, 15.55)	(58.24, 11.08)	(57.68, 8.13)	(51.59, 4.95)
0.6	(0.328, −0.908, 9.387)	(0.324, −0.929, 8.693)	(0.307, −0.855, 8.812)	(0.314, −0.904, 8.309)	(0.300, −0.846, 8.340)
	(34.39, 9.19)	(30.54, 4.11)	(29.16, 3.78)	(27.89, 2.78)	(26.80, 1.80)
0.8	(0.430, −1.417, 7.090)	(0.413, −1.369, 6.848)	(0.407, −1.347, 6.744)	(0.407, −1.360, 6.520)	(0.402, −1.342, 6.409)
	(20.04, 4.08)	(18.35, 1.95)	(17.72, 1.86)	(17.11, 1.37)	(16.59, 0.92)
1.0	(0.514, −1.820, 5.850)	(0.531, −1.928, 5.260)	(0.525, −1.910, 5.171)	(0.524, −1.912, 5.041)	(0.512, −1.862, 5.025)
	(13.23, 2.21)	(12.31, 1.17)	(11.94, 1.12)	(11.61, 0.84)	(11.30, 0.56)
1.5	(0.738, −2.883, 3.820)	(0.757, −2.991, 3.488)	(0.771, −3.064, 3.325)	(0.753, −2.985, 3.338)	(0.746, −2.956, 3.296)
	(6.10, 0.77)	(5.77, 0.42)	(5.64, 0.42)	(5.52, 0.31)	(5.41, 0.21)
2.0	(1.008, −4.156, 2.585)	(1.005, −4.158, 2.455)	(1.013, −4.201, 2.374)	(1.020, −4.239, 2.298)	(1.001, −4.155, 2.307)
	(3.51, 0.38)	(3.35, 0.25)	(3.29, 0.20)	(3.23, 0.15)	(3.18, 0.10)

shifts, i.e. $\delta_{opt} \in \{0.4, 0.8, 1.5, 2.0\}$. It is worth noting that the control statistic of the CUSUM and Shewhart $\bar{X}$ charts are calculated using $n = 5$ observations, since the design specification has been set as $ASN_0 = 5$ for the SPRT chart. For this reason, the Phase-I estimates for the CUSUM and Shewhart $\bar{X}$ charts must be computed using 40 samples, each with subgroup 5, so that the total number of Phase-I observations matches $m = 200$ in the case for the SPRT chart. More details about Phase-I estimation and GICP design for the CUSUM and Shewhart $\bar{X}$ charts can be found in Saleh et al. (2016) and Jardim et al. (2020), respectively. The details are omitted in this paper as they do not constitute the core discussion of our research work.

From Figure 1, it is evident that the GICP-adjusted SPRT chart outperforms both the CUSUM and Shewhart $\bar{X}$ charts in terms of the $CARL_1$, regardless of the size of the mean shift. The GICP-adjusted CUSUM chart is found to perform better than the Shewhart $\bar{X}$ chart for $\delta_{opt} \in \{0.4, 0.8\}$ as expected, but its performances are similar to the Shewhart $\bar{X}$ chart for large shift sizes, i.e. $\delta_{opt} \in \{1.5, 2.0\}$ (Montgomery, 2020). In terms of the $CANOS_1$ performance, one notices that both the GICP-adjusted SPRT and CUSUM charts perform equally well for $\delta_{opt} \in \{0.4, 0.8\}$, although it may be argued that the SPRT chart has a slightly lower median $CANOS_1$ in both cases (see Figure 2).

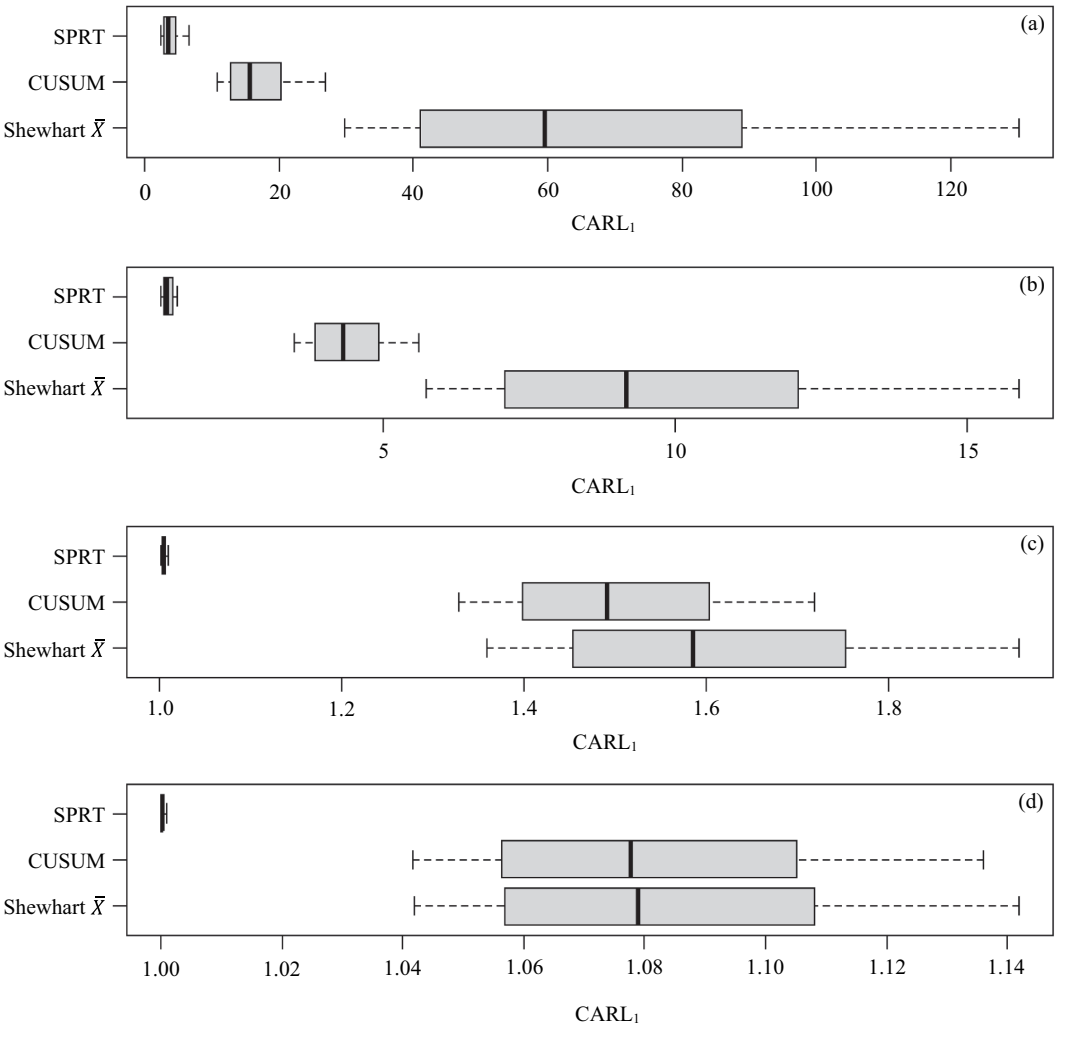

Figure 1. Boxplots showing the 10th, 25th, 50th, 75th, and 90th percentiles of the $CARL_1$ distributions of the AANOS-optimal SPRT, CUSUM, and shewhart $\bar{X}$ charts designed for the shift sizes (a) $\delta_{opt} = 0.4$, (b) $\delta_{opt} = 0.8$, (c) $\delta_{opt} = 1.5$, and (d) $\delta_{opt} = 2.0$, when $m = 200$, $p = 0.05$, and $\varepsilon = 0.2$.

When $\delta_{opt} \in \{1.5, 2.0\}$, the discrepancy between the performances for all the three control charts becomes more visible. The boxplots indicate that the $CANOS_1$ values of the SPRT chart are substantially lower than those of the CUSUM and Shewhart $\bar{X}$ charts under the integrated AANOS optimal-GICP design, further proving the inherent advantage of the SPRT chart over the CUSUM and Shewhart $\bar{X}$ control charts.

It is important to note that all the charting parameters tabulated in Table 2 are ready to be applied in any quality application, given that practitioners have a specialized understanding of the critical shift size to which an out-of-control process is likely to move. Here, we cite an industrial example presented in Hawkins and Olwell (1998). Suppose that gasoline engine is declared as nonconforming if one of its cylinders does not fire. In this case, with some historical experimental evidence, it may be easy for a quality engineer to determine the particular shift in the mean emission of a faulty gasoline engine. If the mean shift size was found to be equal to 1.0, the practitioners may extract the optimal charting parameters of the SPRT chart corresponding to the row $\delta_{opt} = 1.0$ in Table 2, based on the number of Phase-I

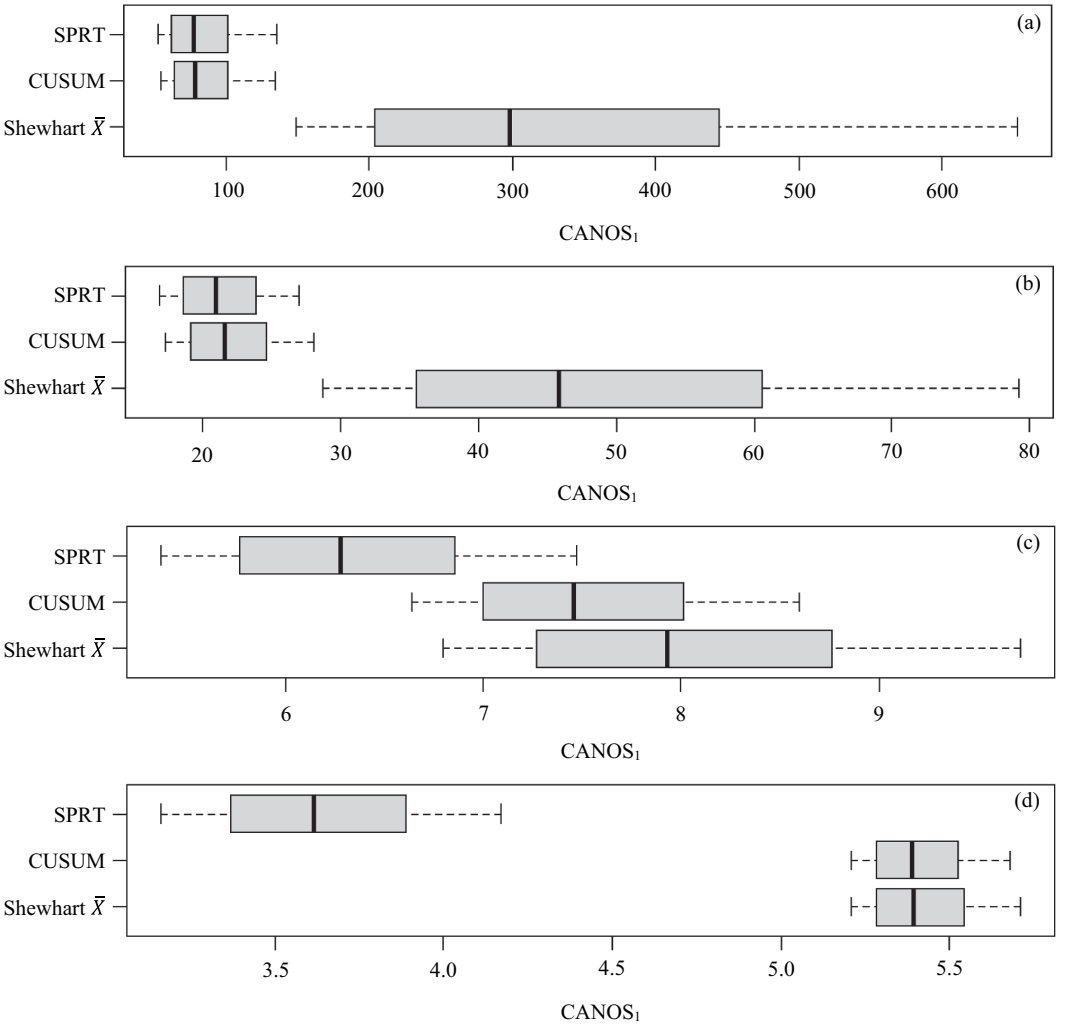

Figure 2. Boxplots showing the 10th, 25th, 50th, 75th, and 90th percentiles of the CANOS$_1$ distributions of the AANOS-optimal SPRT, CUSUM, and shewhart $\bar{X}$ charts designed for the shift sizes (a) $\delta_{opt} = 0.4$, (b) $\delta_{opt} = 0.8$, (c) $\delta_{opt} = 1.5$, and (d) $\delta_{opt} = 2.0$, when $m = 200$, $p = 0.05$, and $\varepsilon = 0.2$.

samples available. However, as stated in Section 1, the assumption that shift sizes are deterministic is unrealistic in many circumstances, since process shifts often occur sparsely in practice. In the subsequent section, we will reveal how the SPRT chart with estimated process parameters can be designed to achieve an optimum performance over a range of shifts, rather than geared towards a particular shift size.

4.2 Minimizing the EAANOS for unknown shift sizes

The optimization model for the SPRT chart with estimated process parameters under unknown shift sizes is given below:

$$\text{Minimize}_{(\gamma,g,h)}\ \text{EAANOS}, \tag{31}$$

subject to constraints Equation (30b) and (30c) from the optimization model in Section 4.1. The procedure for computing the optimal charting parameters is outlined below:

Step 1: Input the values of $m, \tau, \bar{n}, \delta_{\min}, \delta_{\max}, p$, and ε.

Step 2: This step is similar to Step 2 from the optimization model in Section 4.1.

Step 3: Given $\delta_{\min}$ and $\delta_{\max}$, determine the optimal charting parameters (γ, g, h) that yield the smallest EAANOS value. Note that the EAANOS is computed from Equation (28).

Note that in Section 4.1, we have provided a performance comparison between the GICP-adjusted SPRT chart and those of the CUSUM and Shewhart $\bar{X}$ charts. As the SPRT chart is the best performer for each deterministic shift size, it is expected to remain the best performer over a range of shift sizes. Therefore, we shall omit comparisons in this section to avoid presenting duplicated results.

Tables 3 and 4 present the optimal charting parameters of the SPRT chart computed using the above algorithm and their corresponding minimum EAANOS values, for $m \in \{200, 400, 600, 1000, 2000\}$. For each m, we evaluate the (AANOS, SDANOS) values for $\delta \in \{0.0, 0.2, 0.4, 0.6, 0.8, 1.0, 1.5, 2.0\}$. The design specifications are $\tau = 1500$, $\bar{n} = 5$, $\delta_{\min} = 0.1$, $\delta_{\max} = 2.0$, and $\varepsilon \in \{0.0, 0.2\}$. To highlight the differences in the performances across various risk probabilities, we present results for $p = 0.05$ and $p = 0.10$ in Tables 3 and 4, respectively. As a numeric example, when $m = 1000, p = 0.05$, and $\varepsilon = 0.2$, the charting parameters (γ, g, h) of the EAANOS-optimal SPRT chart are $(0.174, -0.131, 14.146)$ with a minimum EAANOS value of 46.277 (see Table 3). Its $(\text{AANOS}_1, \text{SDANOS}_1)$ values for $\delta = 1.5$ are $(11.38, 0.38)$.

From Tables 3 and 4, the optimum EAANOS value decreases as m increases due to a general reduction in the AANOS_1 values over $\delta \in [0.1, 2.0]$. It is also found that increasing the value(s) of p and/or ε leads to improvement in the out-of-control performances. For example, when $m = 400$ and $p = 0.10$, increasing ε from 0% to 20% lowers the EAANOS by almost 13% (i.e. from 66.780 to 58.313) (see Table 4). It is noted that, for moderate and large m, i.e. $m \geq 400$, the optimal SPRT chart with GICP-adjusted limits shows rather similar out-of-control performances to the optimal SPRT chart with unadjusted limits for $\delta \geq 0.6$. For example, when $m = 1000, p = 0.05, \varepsilon = 0.0$ and

Table 3. Optimal charting parameters (γ, g, h), the resulting EAANOS value, and the corresponding (AANOS, SDANOS) values of the SPRT chart with estimated process parameters, designed under the GICP framework, when $p = 0.05$, $\varepsilon = \{0.0, 0.2\}$, $\text{AASN}_0 = 5$, $\tau = 1500$, $\delta_{\min} = 0.1$, $\delta_{\max} = 2.0$, and $m \in \{200, 400, 600, 1000, 2000\}$.

	$m = 200$	$m = 400$	$m = 600$	$m = 1000$	$m = 2000$
	(γ, g, h)	(γ, g, h)	(γ, g, h)	(γ, g, h)	(γ, g, h)
δ	EAANOS (AANOS, SDANOS)	EAANOS (AANOS, SDANOS)	EAANOS (AANOS, SDANOS)	EAANOS (AANOS, SDANOS)	EAANOS (AANOS, SDANOS)
			$\varepsilon = 0.0$		
	(0.422, −1.369, 8.156)	(0.222, −0.361, 13.997)	(0.173, −0.087, 16.328)	(0.171, −0.102, 15.254)	(0.170, −0.117, 14.248)
	204.644	84.950	63.344	51.485	44.160
0.0	(>20,000, >50,000)	(>15,000, >35,000)	(>10,000, >20,000)	(6103.45, 5574.72)	(3526.97, 1806.48)
0.2	(1221.59, 2105.36)	(388.06, 363.16)	(258.26, 143.57)	(216.69, 75.83)	(183.91, 39.47)
0.4	(140.50, 119.19)	(73.34, 19.61)	(71.01, 11.73)	(63.04, 8.06)	(57.92, 5.04)
0.6	(42.36, 15.45)	(37.27, 5.11)	(40.52, 3.90)	(35.75, 2.70)	(33.24, 1.75)
0.8	(22.57, 4.62)	(24.99, 2.39)	(28.39, 2.00)	(24.95, 1.38)	(23.28, 0.90)
1.0	(15.23, 2.20)	(18.82, 1.43)	(21.87, 1.26)	(19.17, 0.86)	(17.92, 0.56)
1.5	(8.41, 0.76)	(11.68, 0.63)	(13.94, 0.59)	(12.18, 0.40)	(11.41, 0.27)
2.0	(5.86, 0.42)	(8.52, 0.39)	(10.28, 0.37)	(8.97, 0.25)	(8.42, 0.17)
			$\varepsilon = 0.2$		
	(0.420, −1.363, 7.810)	(0.226, −0.393, 12.968)	(0.173, −0.096, 15.354)	(0.174, −0.131, 14.146)	(0.169, −0.122, 13.523)
	159.941	71.534	55.954	46.277	40.400
0.0	(>12,000, >30,000)	(>10,000, >20,000)	(8286.72, >10,000)	(4213.97, 3411.00)	(2664.62, 1262.94)
0.2	(957.19, 1472.99)	(335.04, 277.36)	(237.53, 123.60)	(195.92, 64.74)	(167.70, 34.30)
0.4	(125.25, 97.69)	(68.48, 18.10)	(64.63, 11.08)	(58.81, 7.49)	(54.61, 4.69)
0.6	(39.84, 14.04)	(34.87, 4.80)	(36.27, 3.58)	(33.39, 2.52)	(31.50, 1.65)
0.8	(21.51, 4.34)	(23.36, 2.24)	(25.22, 1.81)	(23.29, 1.29)	(22.10, 0.85)
1.0	(14.57, 2.09)	(17.58, 1.34)	(19.35, 1.13)	(17.90, 0.80)	(17.03, 0.54)
1.5	(8.07, 0.72)	(10.91, 0.59)	(12.28, 0.53)	(11.38, 0.38)	(10.86, 0.25)
2.0	(5.63, 0.40)	(7.95, 0.36)	(9.04, 0.33)	(8.38, 0.24)	(8.02, 0.16)

Table 4. Optimal charting parameters (γ, g, h), the resulting EAANOS value, and the corresponding (AANOS, SDANOS) values of the SPRT chart with estimated process parameters, designed under the GICP framework, when $p = 0.10$, $\varepsilon = \{0.0, 0.2\}$, $AASN_0 = 5$, $\tau = 1500$, $\delta_{min} = 0.1$, $\delta_{max} = 2.0$, and $m \in \{200, 400, 600, 1000, 2000\}$.

	$m = 200$	$m = 400$	$m = 600$	$m = 1000$	$m = 2000$
	(γ, g, h)	(γ, g, h)	(γ, g, h)	(γ, g, h)	(γ, g, h)
δ	EAANOS (AANOS, SDANOS)	EAANOS (AANOS, SDANOS)	EAANOS (AANOS, SDANOS)	EAANOS (AANOS, SDANOS)	EAANOS (AANOS, SDANOS)
			$\varepsilon = 0.0$		
	(0.325, −0.886, 9.943)	(0.202, −0.253, 14.013)	(0.172, −0.092, 15.213)	(0.170, −0.105, 14.450)	(0.170, −0.125, 13.719)
	136.471	66.780	54.457	46.532	41.594
0.0	(>18,000, >60,000)	(>10,000, >20,000)	(7608.12, >10,000)	(4362.88, 3617.31)	(2921.18, 1417.69)
0.2	(742.77, 1395.95)	(299.75, 243.60)	(230.96, 117.88)	(195.62, 64.45)	(173.27, 36.07)
0.4	(93.57, 61.73)	(66.94, 16.26)	(63.74, 10.86)	(59.27, 7.47)	(55.67, 4.81)
0.6	(36.21, 9.75)	(35.53, 4.63)	(35.85, 3.53)	(33.81, 2.54)	(32.03, 1.68)
0.8	(21.91, 3.63)	(24.20, 2.24)	(24.96, 1.79)	(23.63, 1.30)	(22.45, 0.87)
1.0	(15.72, 1.95)	(18.38, 1.36)	(19.16, 1.11)	(18.18, 0.81)	(17.29, 0.54)
1.5	(9.25, 0.77)	(11.52, 0.62)	(12.17, 0.52)	(11.57, 0.38)	(11.02, 0.26)
2.0	(6.60, 0.45)	(8.43, 0.38)	(8.96, 0.33)	(8.53, 0.24)	(8.13, 0.16)
			$\varepsilon = 0.2$		
	(0.315, −0.840, 9.758)	(0.181, −0.132, 14.544)	(0.175, −0.122, 14.136)	(0.173, −0.133, 13.502)	(0.171, −0.141, 12.913)
	109.239	58.313	48.672	42.478	38.110
0.0	(>10,000, >40,000)	(9092.65, >15,000)	(5122.47, 6328.07)	(3197.13, 2387.54)	(2207.80, 985.47)
0.2	(592.12, 997.10)	(253.01, 187.92)	(207.96, 98.71)	(178.97, 56.13)	(158.10, 31.42)
0.4	(84.54, 51.03)	(63.75, 14.24)	(59.55, 10.10)	(55.69, 6.99)	(52.33, 4.48)
0.6	(34.31, 8.86)	(35.11, 4.36)	(33.54, 3.31)	(31.80, 2.39)	(30.21, 1.58)
0.8	(21.08, 3.41)	(24.27, 2.17)	(23.34, 1.68)	(22.23, 1.22)	(21.20, 0.82)
1.0	(15.21, 1.85)	(18.56, 1.34)	(17.92, 1.04)	(17.10, 0.76)	(16.34, 0.51)
1.5	(9.02, 0.74)	(11.74, 0.62)	(11.38, 0.49)	(10.88, 0.36)	(10.42, 0.24)
2.0	(6.46, 0.43)	(8.63, 0.39)	(8.38, 0.30)	(8.03, 0.22)	(7.69, 0.15)

$\delta = 0.8$, the $AANOS_1$ (= 24.95) of the SPRT chart with GICP-adjusted limits is reasonably close to that (= 20.23) of the SPRT chart with unadjusted limits (see Tables 1 and 3). While the out-of-control performance of the GICP-adjusted SPRT chart is slightly compromised, its conditional in-control performance is significantly better than the unadjusted SPRT chart. By referring to the same example, we note that the exceedance probability $\Pr(CANOS_0 \geq \tau)$ has increased from 49.68% to 95% after the GICP design is introduced, marking a considerable reduction in its false alarm level. When m is small ($m = 200$), one notices that the $(AANOS_1, SDANOS_1)$ values are all smaller than those for $m \geq 400$ at $\delta \geq 0.8$, whereas at $0.2 \leq \delta \leq 0.6$, the $(AANOS_1, SDANOS_1)$ values are substantially larger for $m = 200$. This is due to the instability in the run-length properties of the SPRT chart when m is small, as inferred by Teoh et al. (2022).

Figure 3 visualizes the distributions of the $CANOS_0$ and $CANOS_1$ of the EAANOS-optimal SPRT chart, when the process parameters are estimated using $m = 200$ Phase-I samples. Five boxplots, each representing the CANOS distributions of the unadjusted SPRT chart and the GICP-adjusted SPRT chart with $p = \{0.05, 0.10\}$ and $\varepsilon \in \{0.0, 0.2\}$, are presented in the same plot. The charting parameters of the traditional SPRT chart can obtained from Table 1, whereas those of the GICP-adjusted SPRT chart can be obtained from Tables 3 and 4. Figure 3(a) shows the in-control distribution, whereas Figures 3(b–e) show the out-of-control distributions for $\delta \in \{0.2, 0.4, 0.6, 0.8\}$. The vertical dotted line in each subplot represents the target ANOS value in the case where process parameters are known (see Table 1, column $m = +\infty$).

From Figure 3(a), it is clear that the in-control performance of the traditional SPRT chart is undesirable, as half of the $CANOS_0$ values are smaller than the nominal $ANOS_0$ value of 1500. After the introduction of the GICP design, the in-control performance of the SPRT chart is improved substantially, although the variability of the $CANOS_0$ values has increased. Here, we argue that the increase in variability is a less concerning issue, as long as the out-of-control performance is not significantly affected by the GICP design (Diko et al., 2019; Kumar, 2022; Teoh et al., 2022). By

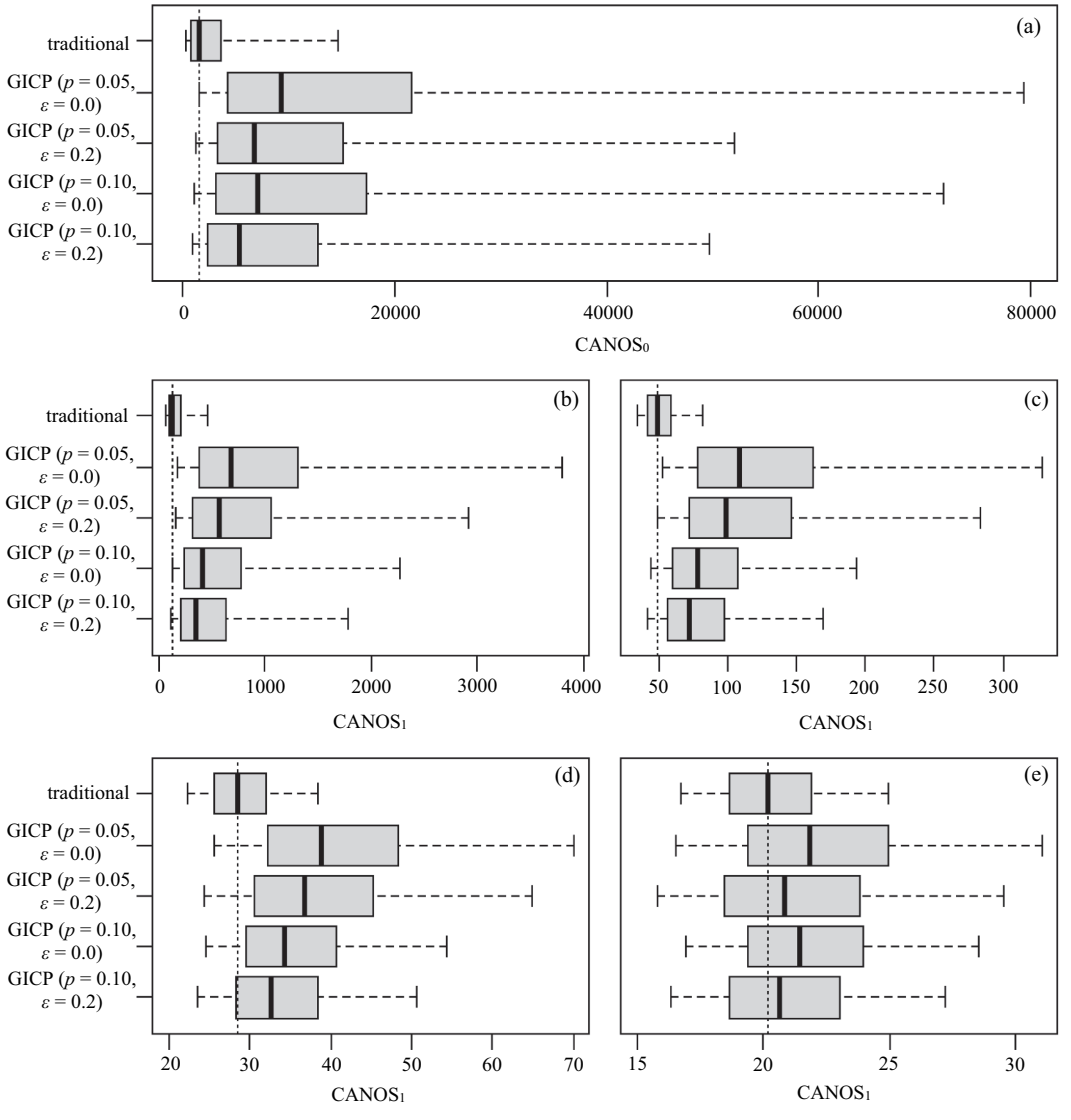

Figure 3. Boxplots showing the 5th, 25th, 50th, 75th, and 95th percentiles of the CANOS distributions evaluated at (a) $\delta = 0.0$, (b) $\delta = 0.2$, (c) $\delta = 0.4$, (d) $\delta = 0.6$, and (e) $\delta = 0.8$ of the optimal SPRT chart with estimated process parameters when $m = 200$.

referring to Figures 3(b–e), we find that the $CANOS_1$ distributions of the GICP-adjusted SPRT chart closely resemble those of the unadjusted SPRT chart for $\delta \geq 0.6$. When $\delta = 0.8$, there is no observable difference between the $CANOS_1$ distributions for all five charts. This indicates a rather good improvement of our proposed integrated optimal-GICP design compared to other GICP designs (see Celano & Chakraborti, 2021; Diko et al., 2019; Hu & Castagliola, 2019), which had only reported similar findings for larger shift sizes (e.g. $\delta \geq 1.0$). Overall, the EAANOS-optimization design is said to complement the GICP model in balancing the in-control and out-of-control performances of the SPRT chart with estimated process parameters. The proposed integrated optimal-GICP design based on the EAANOS metric is robust for mean shifts as small as 0.6.

As the EAANOS-optimization design optimizes the performance of the GICP-adjusted SPRT chart for a range of shift sizes, it is suitable in almost all quality applications. As mentioned by Chong et al. (2022), most industrial processes are affected by external factors

that cause the process to shift randomly. For example, a change in raw materials may affect the output of one stream or a few streams of the production, which can result in mean shifts of unpredictable sizes. As the shift size often varies based on some unknown stochastic model, it is difficult to gauge the actual size of the shift, let alone tuning the charting parameters of the SPRT chart towards a particular δ. A more practical approach is to specify an interval that contains all feasible mean shift sizes of a process, e.g. $\delta \in [0.1, 2.0]$. Hence, the SPRT chart can be designed using the EAANOS-optimization model presented in this section to safeguard against a range of mean shifts, which in this case, has been proven successful in reducing the adverse impact induced by the original GICP design.

5 A real industrial example

This section illustrates an application of the optimal SPRT chart with GICP-adjusted limits for monitoring quality measurements from a wire bonding process. In the microelectronics industry, wire bonding is essential for creating interconnections between integrated circuit chips and substrates. With major advancement in semiconductor technologies, commercial wire pitches are reducing in size, hence greater precision is required to build highly conforming wire loops. A wire loop height that is too low or too high may impact the stability of a bonding machine and/or the pull force readings. It is, therefore, crucial to monitor loop height measurements during the wire bonding process to ensure appropriate wire formation.

The loop height measurements used in this example are obtained from an optoelectronic device manufacturing company. The company currently supplies a particular processor chip to a renowned smartphone manufacturer, playing the role as one of its biggest and most crucial suppliers. Recently, the smartphone manufacturer plans to launch a new device model, which offers a promising improvement in the device's network connectivity, camera sensors, as well as battery efficiency. To account for the product change, the optoelectronic device manufacturing company decides to establish a new production line for fabricating the modified processor chip package. The new package is not only smaller in size, but also incorporates advanced architecture that enhances the overall performance of the smartphone. As the production line is relatively new, there are limited historical data for estimating the parameters of the loop height measurements. In our example, we have collected $m = 200$ Phase-I loop height measurements $(Y_1, \ldots, Y_{200})$ from the wire bonding process of the new processor chip package. All loop heights are measured in one-thousandth of an inch (mils). To check the stability of the Phase-I samples, we use the classical average moving range (AMR) chart for individual measurements (see Fry et al., 2012; Montgomery, 2020). The lower (LCL) and upper (UCL) control limits of the AMR chart are computed as

$$\hat{\mu}_0 \pm (3\sqrt{\pi}/2)\overline{MR} = (6.382, 8.878), \quad \text{where} \quad \hat{\mu}_0 = \sum_{\varphi=1}^{200} Y_\varphi/200 = 7.630 \text{ mils and}$$

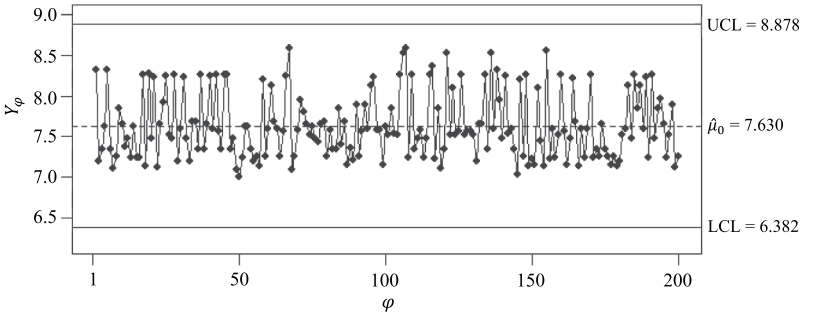

Figure 4. The Phase-I AMR control chart for $m = 200$ loop height measurements.

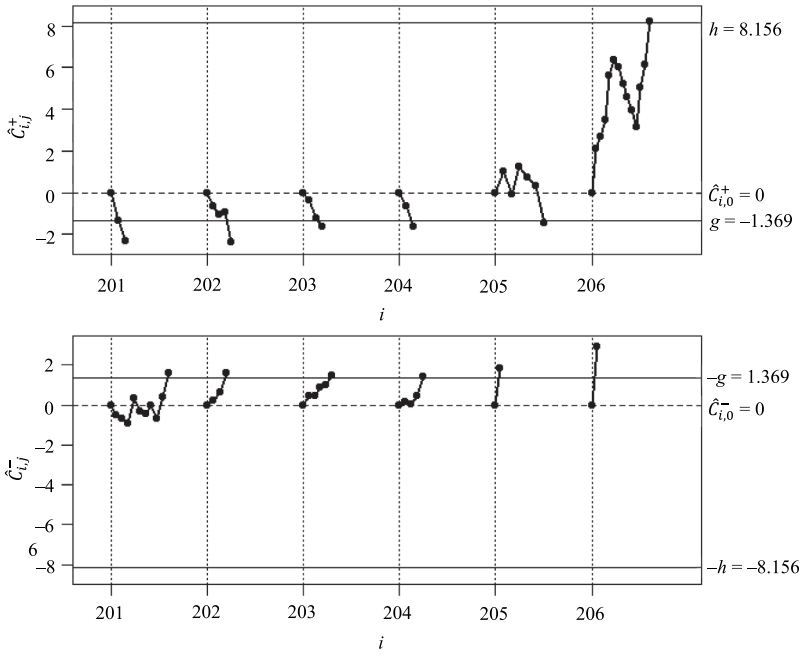

Figure 5. The Phase-II upper and lower-sided SPRT chart with estimated process parameters for monitoring loop height measurements.

$\overline{MR} = \sum_{\varphi=1}^{199} |Y_{\varphi+1} - Y_{\varphi}|/199 = 0.469$ mils. The Phase-I AMR control chart for the Phase-I dataset is shown in Figure 4. From the chart, we confirm that the samples come from an in-control distribution, and the process parameters are estimated using Equations (13) and (14) as $\hat{\mu}_0 = 7.630$ mils and $\hat{\sigma}_0 = 0.402$ mils, respectively.

In Phase-II process monitoring, we select the EAANOS-optimal SPRT chart with GICP-adjusted limits designed corresponding to $\tau = 1500, \text{AASN}_0 = 5, \delta_{\min} = 0.1, \delta_{\max} = 2.0, p = 0.05$, and $\varepsilon = 0.0$. The optimal charting parameters can be quoted directly from Table 3 as $(\gamma, g, h) = (0.422, -1.369, 8.156)$. Figure 5 displays the upper and lower-sided SPRT charts with estimated process parameters for monitoring the Phase-II loop height measurements. The upper- and lower-sided charting statistics have been calculated using Equations (15) and (16), respectively. From Figure 5, the process is declared as in-control for the first five sampling times ($i = 201$–205), with the number of observations inspected equal to 10, 4, 5, 4, 6, respectively. When the sixth SPRT is sampled, $C^{+}_{6,13}$ increases beyond h after 13 measurements are taken. An out-of-control signal is emitted, and investigative plans are conducted to identify the root cause of the shift. The number of observations to signal of the two one-sided SPRT schemes is reported as 42 (= 10 + 4 + 5 + 4 + 6 + 13).

6 Concluding remarks

In this paper, we extend the work of Teoh et al. (2022) by developing two new optimal designs of the SPRT chart with estimated process parameters based on the AANOS and EAANOS metrics. Both optimal designs are proposed in this paper as they better exploit the benefits of the SPRT chart, which possesses the VSS feature. In particular, the AANOS- and EAANOS-optimization algorithms seek the smallest product of AASN_1 and AARL_1, allowing for a high detection speed and high out-of-control sampling efficiency at the same time. Unlike traditional chart designs, our proposed GICP framework ensures that all the in-control performances obtained by practitioners meet the minimum threshold

with a very high probability (90% or 95%). As a result, the levels of harmful false alarms are substantially reduced, and the long-term efficiency of the production line can be maintained at a satisfactory level. We also demonstrate that the optimization design is effective in lowering the discrepancy between the out-of-control performances of the traditional and GICP-adjusted SPRT charts. Using a moderate number of Phase-I samples (e.g. $m = 200$), it is possible to optimize the performance of the SPRT chart for a particular shift (or over a range of shifts), while keeping the in-control performance at a satisfactory level. Results also show that the integrated optimal-GICP design is robust towards parameter estimation for $\delta \geq 0.6$. Besides, practitioners are encouraged to tune the rigidity of the GICP strategy according to the appropriate culture practised by the company. This is done by adjusting p and/or ε in the EPC formula to degrade/tighten the in-control standards. We also publish tables of charting parameters for the optimal SPRT chart that are directly applicable for industrial use. In the future, researchers can develop optimal designs for the SPRT chart with estimated process parameters based on the median run length or median number of observations to signal. As the median provides a more realistic representation of a skewed random variable (such as the run length), such designs can be appealing to quality engineers and may shape a new perspective on the evaluation of the performances of the SPRT chart with estimated process parameters.

Disclosure statement

No potential conflict of interest was reported by the author(s).

Funding

This work was supported by the Ministry of Higher Education (MOHE) Malaysia and Heriot-Watt University Malaysia under the Fundamental Research Grant Scheme (FRGS), no. FRGS/1/2021/STG06/HWUM/02/1.

Notes on contributors

Jing Wei Teoh is a PhD student in the School of Mathematical and Computer Sciences, Heriot--Watt University Malaysia (HWUM). He holds a B.Sc. (Hons) in Actuarial Science from HWUM. His research interest is in statistical process control.

Wei Lin Teoh is an Assistant Professor in the School of Mathematical and Computer Sciences, HWUM. She received her PhD in Applied Statistics in 2013 from Universiti Sains Malaysia (USM). Her research interest is in statistical process control. She has authored/co-authored more than 80 papers in peer-reviewed international journals and proceedings of international conferences, including Q1 journals indexed in the Web of Science (WoS) database. She serves as an Associate Editor of the *Journal of Statistical Computation and Simulation*. She holds the role of a visiting researcher and member of the International Chair in Data Science & Explainable Artificial Intelligence at the International Research Institute for Artificial Intelligence and Data Science, situated at Dong A University in Danang, Vietnam.

Michael B. C. Khoo is a Professor in the School of Mathematical Sciences, USM. He received his PhD in Applied Statistics in 2001 from USM. He specializes in Statistical Quality Control. He has published numerous papers in international journals indexed in WoS database. He has also reviewed numerous papers for journals indexed in the WoS database.

Kim Phuc Tran is currently a Senior Associate Professor (Maîtrede Conférences HDR, equivalent to a UK Reader) of Artificial Intelligence and Data Science at the ENSAIT and the GEMTEX laboratory, University of Lille, France. He received an Engineer's degree and a Master of Engineering degree in Automated Manufacturing. He received his PhD in Automation and Applied Informatics from the University of Nantes, and an HDR (Doctor of Science or Dr. habil.) in Computer Science and Automation from the University of Lille, France. His research deals with Real-time Anomaly Detection with Machine Learning with applications, Decision Support Systems with Artificial Intelligence, and Enabling Smart Manufacturing with IIoT, Federated learning, and Edge computing. He has published more than 64 papers in peer-reviewed international journals and proceedings of international conferences. He edited 3 books with Springer Nature and Taylor & Francis. He is the Associate Editor, Editorial Board Member, and Guest Editor for several international journals such as IEEE Transactions on Intelligent Transportation Systems and Engineering Applications of Artificial Intelligence. He has supervised 9 PhD students and 3 Postdocs. In

addition, as the project coordinator (PI), he is conducting 1 regional research project about Healthcare Systems with Federated Learning. He has been or is involved (co-PI or member) in 8 national and European projects. He is an expert and evaluator for the Research and Innovation program of the Government of the French Community, Belgium. He received the Award for Scientific Excellence (Prime d'Encadrement Doctoral et de Recherche) given by the Ministry of Higher Education, Research and Innovation, France for 4 years from 2021 to 2025 in recognition of his outstanding scientific achievements. From 2017 until now, he has been the Senior Scientific Advisor at Dong A University and the International Research Institute for Artificial Intelligence and Data Science (IAD), Danang, Vietnam where he has held the International Chair in Data Science and Explainable Artificial Intelligence.

Ming Ha Lee received her B.Tech. degree from USM, her M.Sc. degree from Universiti Putra Malaysia, and her PhD degree from USM. She is a senior lecturer with the Faculty of Engineering, Computing and Science, Swinburne University of Technology Sarawak Campus, Malaysia.

ORCID

J.W. Teoh http://orcid.org/0000-0001-7148-0038
W.L. Teoh http://orcid.org/0000-0003-4715-1490
Michael B.C. Khoo http://orcid.org/0000-0002-3245-1127
K.P. Tran http://orcid.org/0000-0002-6005-1497
M.H. Lee http://orcid.org/0000-0003-2096-5865

References

Calzada, M. E., & Scariano, S. M. (2013). The synthetic *t* and synthetic EWMA *t* charts. *Quality Technology & Quantitative Management*, *10*(1), 37–56. https://doi.org/10.1080/16843703.2013.11673307

Capizzi, G., & Masarotto, G. (2020). Guaranteed in-control control chart performance with cautious parameter learning. *Journal of Quality Technology*, *52*(4), 385–403. https://doi.org/10.1080/00224065.2019.1640096

Celano, G., & Chakraborti, S. (2021). A distribution-free shewhart-type Mann–Whitney control chart for monitoring finite horizon productions. *International Journal of Production Research*, *59*(20), 1–18. https://doi.org/10.1080/00207543.2020.1802079

Chong, Z. L., Tan, K. L., Khoo, M. B. C., Teoh, W. L., & Castagliola, P. (2022). Optimal designs of the exponentially weighted moving average (EWMA) median chart for known and estimated parameters based on median run length. *Communications in Statistics-Simulation and Computation*, *51*(7), 3660–3684. https://doi.org/10.1080/03610918.2020.1721539

Chou, Y. M., Mason, R. L., & Young, J. C. (2006). The SPRT control chart for standard deviation based on individual observations. *Quality Technology & Quantitative Management*, *3*(3), 335–345. https://doi.org/10.1080/16843703.2006.11673119

Deore, R. E., Mahadik, S. B., & Godase, D. G. (2023). The two-sided SPRT sign charts. *Quality and Reliability Engineering International*. In Press. https://doi.org/10.1002/qre.3451

Diko, M. D., Chakraborti, S., & Does, R. J. M. M. (2019). An alternative design of the two-sided CUSUM chart for monitoring the mean when parameters are estimated. *Computers & Industrial Engineering*, *137*(11), 106042. https://doi.org/10.1016/j.cie.2019.106042

Fry, D. E., Pine, M., Jones, B. L., & Meimban, R. J. (2012). Control charts to identify adverse outcomes in elective colon resection. *The American Journal of Surgery*, *203*(3), 392–396. https://doi.org/10.1016/j.amjsurg.2011.09.011

Godase, D. G., & Mahadik, S. B. (2019). The SPRT control chart for process dispersion. *Quality and Reliability Engineering International*, *35*(6), 1878–1889. https://doi.org/10.1002/qre.2481

Godase, D. G., Mahadik, S. B., & Rakitzis, A. C. (2022). The SPRT control charts for the Maxwell distribution. *Quality and Reliability Engineering International*, *38*(4), 1713–1728. https://doi.org/10.1002/qre.3047

Gong, P., Xia, Q., Xuan, J., Saghir, A., & Guo, B. (2023). Design of Shewhart-type control charts with estimated parameter for the Rayleigh distribution using frequentist and Bayesian approaches. *Quality Technology & Quantitative Management*, *20*(4), 450–467. https://doi.org/10.1080/16843703.2022.2124778

Hawkins, D. M., & Olwell, D. H. (1998). *Cumulative sum charts and charting for quality improvement*. Springer Science + Business Media.

Hu, X., & Castagliola, P. (2019). A re-evaluation of the run rules $\bar{X}$ chart when the process parameters are unknown. *Quality Technology & Quantitative Management*, *16*(6), 696–725. https://doi.org/10.1080/16843703.2018.1513826

Jardim, F. S., Chakraborti, S., & Epprecht, E. K. (2020). Two perspectives for designing a phase II control chart with estimated parameters: The case of the shewhart $\bar{X}$ chart. *Journal of Quality Technology*, *52*(2), 198–217. https://doi.org/10.1080/00224065.2019.1571345

Katebi, M., & Rahim, A. (2021). Optimal economic statistical design of adaptive attribute control charts for monitoring three level products. *Quality Technology & Quantitative Management*, *18*(5), 597–619. https://doi.org/10.1080/16843703.2021.1930344

Khusna, H., Mashuri, M., Ahsan, M., Suhartono, S., & Prastyo, D. D. (2020). Bootstrap-based maximum multivariate CUSUM control chart. *Quality Technology & Quantitative Management*, *17*(1), 52–74. https://doi.org/10.1080/16843703.2018.1535765

Kumar, N. (2022). Statistical design of phase II exponential chart with estimated parameters under the unconditional and conditional perspectives using exact distribution of median run length. *Quality Technology & Quantitative Management*, *19*(1), 1–18. https://doi.org/10.1080/16843703.2021.1972515

Mahadik, S. B., & Godase, D. G. (2023). The SPRT sign chart for process location. *Communications in Statistics-Theory and Methods*, *52*(7), 2276–2290. https://doi.org/10.1080/03610926.2021.1949474

Malela-Majika, J. C., Shongwe, S. C., Aslam, M., Chong, Z. L., & Rapoo, E. M. (2021). Distribution-free double-sampling precedence monitoring scheme to detect unknown shifts in the location parameter. *Quality and Reliability Engineering International*, *37*(8), 3580–3599. https://doi.org/10.1002/qre.2935

Montgomery, D. C. (2020). *Introduction to statistical quality control*. John Wiley & Sons.

Moustakides, G. V. (1986). Optimal stopping times for detecting changes in distributions. *The Annals of Statistics*, *14*(4), 1379–1387. https://doi.org/10.1214/aos/1176350164

Mustafa, F., Khan Sherwani, R. A., & Raza, M. A. (2023). A progressive mean control chart for dispersed count data considering tail behavior. *Quality Technology & Quantitative Management*. In Press. 1–20. https://doi.org/10.1080/16843703.2023.2246768

Ou, Y., Wu, Z., Chen, S., & Lee, K. M. (2010). An improved SPRT control chart for monitoring process mean. *The International Journal of Advanced Manufacturing Technology*, *51*(9–12), 1045–1054. https://doi.org/10.1007/s00170-010-2675-6

Ou, Y., Wu, Z., Lee, K. M., & Chen, S. (2012). An optimal design algorithm of the SPRT chart for minimizing weighted ATS. *International Journal of Production Economics*, *139*(2), 564–574. https://doi.org/10.1016/j.ijpe.2012.05.031

Rasay, H., & Alinezhad, E. (2022). Developing an adaptable sequential probability ratio test applicable for lifetime analysis of different continuous distributions. *Quality Technology & Quantitative Management*, *19*(4), 511–530. https://doi.org/10.1080/16843703.2021.2020954

Saleh, N. A., Mahmoud, M. A., Jones-Farmer, L. A., Zwetsloot, I., & Woodall, W. H. (2015). Another look at the EWMA control chart with estimated parameters. *Journal of Quality Technology*, *47*(4), 363–382. https://doi.org/10.1080/00224065.2015.11918140

Saleh, N. A., Zwetsloot, I. M., Mahmoud, M. A., & Woodall, W. H. (2016). CUSUM charts with controlled conditional performance under estimated parameters. *Quality Engineering*, *28*(4), 402–415. https://doi.org/10.1080/08982112.2016.1144072

Sarmiento, M. G. C., Jardim, F. S., Chakraborti, S., & Epprecht, E. K. (2022). Design of variance control charts with estimated parameters: A head to head comparison between two perspectives. *Journal of Quality Technology*, *54*(3), 249–268. https://doi.org/10.1080/00224065.2020.1834892

Stoumbos, Z. G., & Reynolds, M. R., Jr. (1997). Control charts applying a sequential test at fixed sampling intervals. *Journal of Quality Technology*, *29*(1), 21–40. https://doi.org/10.1080/00224065.1997.11979722

Teoh, J. W., Teoh, W. L., Khoo, M. B. C., Castagliola, P., & Moy, W. H. (2022). On designing an optimal SPRT control chart with estimated process parameters under guaranteed in-control performance. *Computers & Industrial Engineering*, *174*(12), 108806. https://doi.org/10.1016/j.cie.2022.108806

Yeong, W. C., Tan, Y. Y., Lim, S. L., Khaw, K. W., & Khoo, M. B. C. (2023). Variable sample size and sampling interval (VSSI) and variable parameters (VP) run sum charts for the coefficient of variation. *Quality Technology & Quantitative Management*, *21*(2), 177–199. In Press. https://doi.org/10.1080/16843703.2023.2177812

You, H. W., Khoo, M. B. C., Lee, M. H., & Castagliola, P. (2015). Synthetic double sampling $\bar{X}$ chart with estimated process parameters. *Quality Technology & Quantitative Management*, *12*(4), 579–604. https://doi.org/10.1080/16843703.2015.11673437